78-503

A Theoretical Technique for Analyzing Aeroelastic Stability of Bearingless Rotors

Dewey H. Hodges*
U.S. Army R & T Laboratories (AVRADCOM), Ames Research Center, Moffett Field, Calif.

A technique is introduced for aeroelastic stability analysis of certain hingeless helicopter rotors termed bearingless because of their lack of a pitch-change bearing. The rotor is modeled as three or more rigid blades, each joined to the hub by means of a flexible appendage known as the flexbeam or strap. The pitch-control system twists the flexbeam to provide blade pitch change. The analysis is capable of treating effects of several different pitch-control configurations, geometic nonlinearities associated with the equilibrium deflected shape of the flexbeam, and the built-in angular offsets of the flexbeam and blade. Numerical results are presented for a variety of system parameters. The stability of the system in both hub-fixed motion and coupled rotor-body motion is considered. System parameters can be chosen to stabilize most soft in-plane configurations for the hub-fixed case. The same parameters will also, under certain conditions, stabilize the coupled rotor-body system in hovering flight (air resonance). When the rotorcraft is in ground contact, however, at zero thrust, it appears that these parameters are not as effective in stabilizing the system (ground resonance).

Nomenclature

$[A]$ = inertia matrix, Eq. (6)
b = number of blades
$[B]$ = damping and gyroscopic matrix, Eq. (6)
$[C]$ = stiffness matrix, Eq. (6)
$\mathfrak{F}$ = function to be minimized to produce flexbeam equilibrium deflections
$[F]$ = flexbeam flexibility matrix
F = steady component of F_k, N
F_k = force acting on the kth blade
$\tilde{F}_{uk}, \tilde{F}_{vk}, \tilde{F}_{wk}$ = perturbation components of force in the direction of u,v,w, respectively, acting at the flexbeam tip, N
h = height of rotor-hub center above aircraft reference center, m
I_x, I_y = body mass moment of inertia at the body mass center for axes N_A and N_B, respectively, kg-m^2
L = blade, length, m
ℓ = flexbeam length, m
M = steady component of M_k, N-m
M_k = moments exerted on the kth blade, N-m
$\tilde{M}_{\zeta k}, \tilde{M}_{\beta k}, \tilde{M}_{\theta k}$ = perturbation components of moments in the direction of ζ,β,θ, respectively, acting at the flexbeam tip, N-m
m = mass of one rotor blade, kg
m_f = mass of the fuselage, kg
n_1^k, n_2^k, n_3^k = coordinate system fixed at the kth flexbeam root
n_x^k, n_y^k, n_z^k = coordinate system fixed at the kth deformed flexbeam tip
u,v,w = steady components of u_k, v_k, and w_k, m
u_k, v_k, w_k = axial, chordwise, and flapwise deflections, respectively, of the kth flexbeam tip, m
u_1, v_1, w_1
u_2, v_2, w_2 = parameters describing the location of the pitch link/swashplate junction and the snubber link/ground junction, m
X, Y = time integrals of body velocity components in N_A and N_B directions, respectively, m/s
$\{x\}$ = column vector with elements: $u_c, u_s, v_c, v_s, w_c, w_s, \zeta_c, \zeta_s, \beta_c, \beta_s, \theta_c, \theta_s, X, Y, \Phi_x, \Phi_y$
x_1, y_1, z_1,
x_2, y_2, z_2 = parameters describing the location of the pitch link/pitch arm junction and the snubber link/snubber arm junction, m
z = vertical distance from aircraft reference center to body mass center, positive when body mass center is below reference center, m
β,ζ,θ = steady components of β_k, ζ_k, and θ_k, rad
$\beta_b, \zeta_b, \theta_b$ = built-in flap, lead, and pitch angles of the blade with respect to the flexbeam, rad
$\beta_f, \zeta_f, \theta_f$ = built-in flap, lead, and pitch angles of the flexbeam with respect to the hub, rad
$\beta_k, \zeta_k, \theta_k$ = elastic flap, lead, and pitch angles of the kth flexbeam tip, rad
ϵ = perturbation of flexbeam tip loads
σ = real part of eigenvalue, rad/s
Φ_x, Φ_y = time integrals of body angular velocity components in N_A and N_B directions, respectively, rad
ψ_k = azimuth angle of kth blade, rad
Ω = rotor angular velocity, rad/s
$\bar{\Omega}$ = Ω/Ω_0
Ω_0 = nominal rotor angular velocity, rad/s
ω = modal frequency, rad/s

Subscripts

$(\,)_R$ = value of $(\,)$ at the flexbeam root
$(\,)_t$ = assumed value for $(\,)$ in equilibrium deflection scheme

Superscripts

$(\tilde{\ })$ = unsteady component of $(\,)$
$(\bar{\ })$ = $(\,)/\ell$, applied to pitch-control geometry only

Received Jan. 26, 1978; presented as Paper 78-503 at the AIAA/ASME 19th Structures, Structural Dynamics and Materials Conference, Bethesda, Md., April 3-5, 1978; revision received Oct. 16, 1978.

Index categories: Structural Dynamics; Helicopters; Aeroelasticity and Hydroelasticity.

*Research Scientist, Rotorcraft Dynamics Division, Aeromechanics Laboratory. Associate Fellow AIAA.

Introduction

THE helicopter industry has devoted considerable attention during the past two decades to the development of hingeless rotors. Hingeless rotors have distinct advantages over the more common hinged (articulated) rotors; these include lighter weight, mechanical simplicity, and increased control power. Even though the hinges associated with blade flap and lead-lag motions are eliminated, pitch bearings near the blade root are retained to accommodate blade pitch changes. Because of weight and blade stress considerations, main rotor designs have been mostly soft in-plane; that is, the blade lead-lag frequency is less than the rotor angular speed. Such designs, however, are susceptible to aeromechanical instabilities in the air and on the ground, commonly known as air and ground resonance.[1-5] In these instabilities, the low-frequency rotor modes interact with rigid-body fuselage motions to produce instabilities near the coalescence of frequencies.

In recent years, there have been efforts to develop hingeless rotors without pitch bearings to further reduce mechanical complexity and weight. These rotors, called bearingless rotors, rely on a torsionally soft portion of the blade called the flexbeam (or flex strap) that is twisted by the pitch-control system to provide change in pitch. Several variations of the pitch-control geometry have been designed within the helicopter industry.[6-10] Although the aeroelastic stability characteristics of hub-fixed motion for hingeless rotor blades are reasonably well understood,[11,12] the same is not true for bearingless rotors. Furthermore, preventing air and ground resonance instabilities in aircraft with either hingeless or bearingless rotors remains a difficult design problem.

Some production helicopters with hingeless rotors rely on auxiliary lead-lag dampers to suppress air and ground resonance instabilities. One reason that this breach in mechanical simplicity has been necessary is believed to be the lack of suitable analytical capability. Analytical treatment of such configurations has been limited primarily to equivalent-hinge, spring-restrained, rigid-blade models for the rotor blades.[1-5] While such modeling is adequate for some configurations, a separate analysis is necessary to properly define the aeroelastic couplings which arise from blade elastic deflections, blade and flexbeam angular offsets, and pitch-control geometry. This is particularly undesirable for bearingless rotors where the couplings vary significantly as a function of operating condition. For example, when the rotor is at high thrust the flexbeam may be highly twisted; whereas, at low thrust it may be untwisted. With previous analytical capability, the skillful analyst could, after trial and error, reproduce some trends of experimental data. But reliable treatment of wide varieties of configurations is not possible in this manner.

An elastic blade model formulation may present other difficulties. For a bearingless rotor, the coupled mode-shape changes as a function of operating condition and additional problems arise because of the structural redundancy associated with the pitch-control geometry.[13] An analysis that possesses the simplicity of a rigid-blade model but includes treatment of the flexbeam and pitch-control system would be a useful tool. Such an analysis has been developed and is described in this paper.

Only an outline of the analysis is presented here. The full derivation, including the equations of motion, is given in Ref. 14. The analysis is based on modeling the rotor with three or more rigid blades attached to the hub by flexible appendages which simulate the flexbeam portion of a bearingless rotor blade. The fuselage is modeled as a rigid body, as in Ref. 5. Hub-fixed dynamic behavior may be studied by simply deleting fuselage degrees of freedom.

An iterative structural analysis, including geometric nonlinearities, leads to the solution for the equilibrium deflected shape of the flexbeam. A numerical perturbation scheme is then used to obtain the stiffness matrix for the tip of the flexbeam. The linearized perturbation forces and moments associated with the flexbeam structure, body springs and dampers, the pitch-control geometry, and inertial, gravitational, and aerodynamic loadings, when combined, yield a system of linear, homogeneous, ordinary differential equations. Eigenvalues are obtained to assess the system stability for various pitch-control configurations, angular offsets of the flexbeam and blade, thrust, and rotor angular speed. Both hub-fixed and coupled rotor-body results are presented.

Analytical Model

In this section, the analytical model used to represent an actual helicopter is described. Only the elements of the model believed essential for studying air and ground resonance are retained. The fuselage is assumed to be a rigid body. When in contact with the ground, the fuselage is supported by a system of springs and dampers to simulate the restraint to fuselage motion in an actual helicopter due to the landing gear system. When airborne in hovering flight the aircraft is unrestrained elastically. The rotor consists of three or more rigid blades attached to the hub by means of slender elastic beam segments. These beam segments represent the flexbeam or strap of a bearingless rotor.

A schematic of the fuselage is shown in Fig. 1. The hub, mast, and landing gear are all included in the mass and inertia of the fuselage. The total fuselage mass is m_f and the moments of inertia for the mass center of the fuselage are I_x and I_y, respectively, for the X and Y directions. The aircraft reference center is a distance z above the body mass center and a distance h below the hub center. For air resonance and ground resonance, in hover and on the ground, respectively, vertical translation and yaw rotation of the body are insignificant. In this analysis, therefore, only longitudinal translation X, lateral translation Y, body roll Φ_x, and body pitch Φ_y are included. The landing gear provides stiffness and damping restraining X, Y, Φ_x, Φ_y motion depending on the landing gear geometry.

The rotor blades are attached to the hub and rotate at constant angular velocity Ω. The azimuth angle of the kth blade is $\psi_k = \Omega t + (2\pi/b)(k-1)$. The blade axis system and built-in angular offsets for the kth blade are illustrated in Fig. 2. A simplified schematic of the rotor blade model is shown in Fig. 3 with all deformations and built-in angular offsets equal to zero. Details of the pitch-control systems are to be discussed.

The pitch angle of the rotor blade may be changed by various types of control systems. In order to model several representative types of pitch-control systems, four model configurations were selected, schematically shown in Fig. 4. Case I, for which there is no control system, is the simplest.

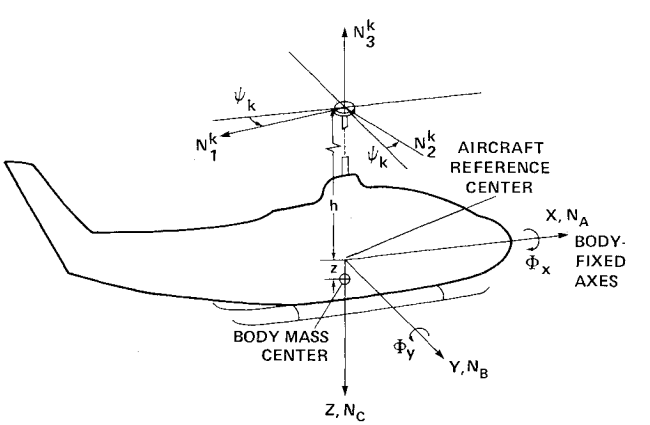

Fig. 1 Rotorcraft fuselage model.

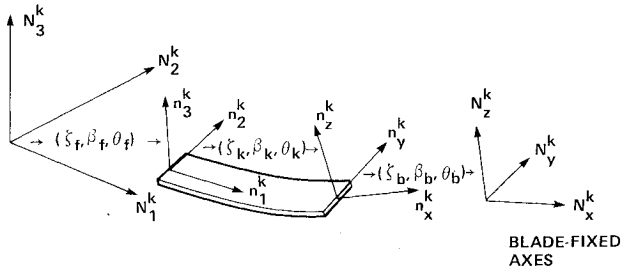

Fig. 2 Rotating rotor blade coordinate system.

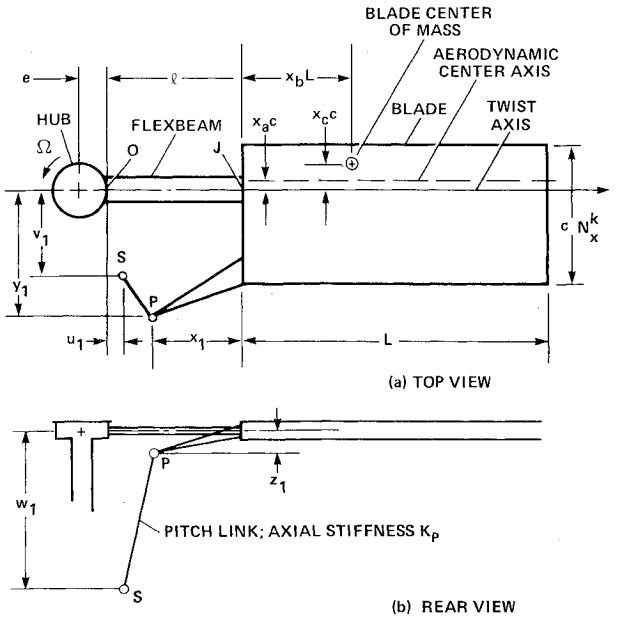

Fig. 3 Rotor blade configuration.

The pitch angle is changed by changing the built-in angles θ_f and θ_b. This configuration corresponds to an experimental rotor set up to operate only at discrete pitch angles or an operational rotor with a disabled control system. Case II has a torque tube that is assumed to be torsionally stiff enough to twist the flexbeam, but flexible enough in bending to impose a pure twisting moment on the flexbeam tip. This configuration corresponds to that of Ref. 10 and also, approximately, to configurations with a pinned-pinned torque tube in Ref. 6. Case III corresponds to configurations with a pitch link and cantilevered pitch arm described in Refs. 6, 8, and 9. Pitch change is often accompanied by bending deflections and vice versa, leading to large pitch-bending couplings for some configurations. Case IV is identical to case III, except that a snubber is added. The snubber in case IV is modeled as an additional, nonfunctioning pitch-link/pitch-arm assembly to reduce pitch-bending couplings. The pitch link is connected to the rotating swashplate, but the snubber link is connected to a point stationary in the rotating system. A configuration similar to this is described in Ref. 7. A detailed schematic of pitch- (or snubber-) link geometry is shown in Fig. 3. The coordinates of point S are measured from point $O(n_1^k,n_2^k,n_3^k$ system) and the coordinates of point J are measured from point $P(n_x^k,n_y^k,n_z^k$ system). Reference 14 discusses the analytical model in more detail.

Theoretical Analysis

A complete derivation of the equations of motion used in this analysis is beyond the scope of this paper, but may be found in Ref. 14. This analysis is based on the set of generalized forces due to inertia, gravity, body springs and dampers (when the aircraft is in ground contact), quasisteady aerodynamics, and the flexbeam structure. All of these generalized forces (except those due to flexbeam structural loads) are written exactly, for arbitarily large deflections, and analytically linearized about equilibrium. The geometric nonlinearities in the flexbeam deflections are treated exactly for an Euler-Bernoulli beam segment. The equilibrium-deflected shape is obtained iteratively and the flexbeam structural loads for small perturbation deflections are found through numerical perturbation of the equilibrium solution. These steps and a suitable transformation lead to a system of linear, constant-coefficient, homogeneous, ordinary differential equations.

Generalized Forces

In addition to the fuselage rigid-body degrees of freedom X,Y,Φ_x,Φ_y already described, the six rigid-body degrees of freedom of the kth blade in the rotating system may be expressed as: 1) three translations of the point P corresponding to the n_1^k,n_2^k,n_3^k axis system, u_k,v_k,w_k, respectively, and 2) three rotations, ζ_k,β_k,θ_k, lead, flap, and pitch angles, respectively, of the blade (beginning with ζ_k about the n_3^k axis,

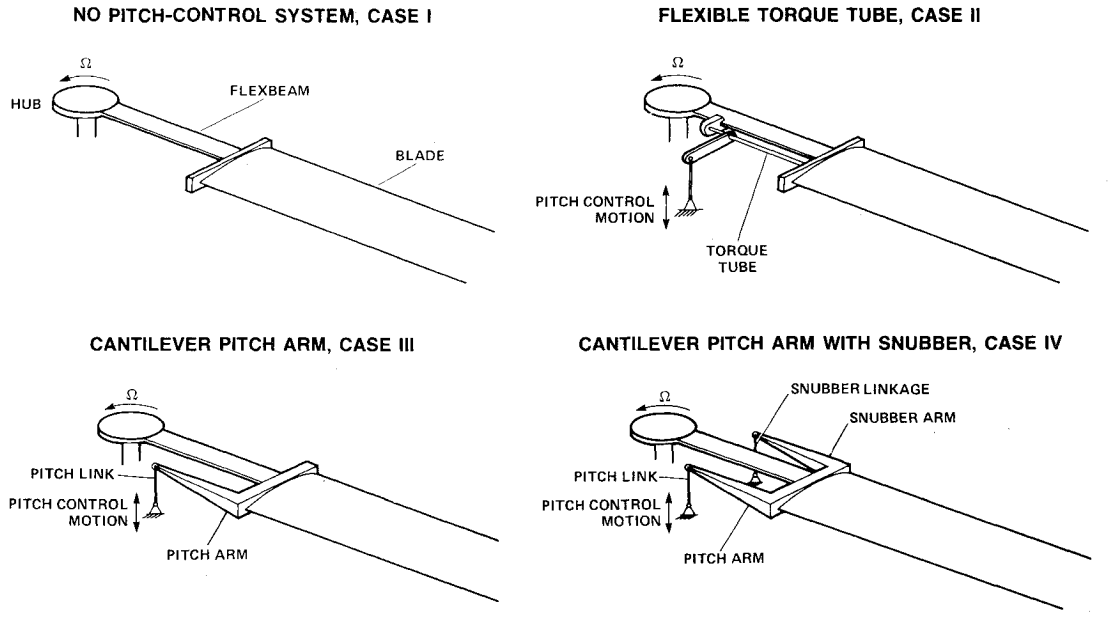

Fig. 4 Various pitch-control geometries treated in the analysis.

β_k about the axis $n_1^k \sin\zeta_k - n_2^k \cos\zeta_k$, and θ_k about the n_x^k axis). Such a sequence is noted only for the purpose of definition; obviously, for an elastic flexbeam the choice of the sequence of angles is entirely arbitrary.

Using a Lagrangian form of D'Alembert's principle,[15] exact expressions for the generalized forces due to inertia, gravity, body springs, the pitch-control systems, and quasisteady airloads[16] are derived in Ref. 14. The total forces acting along the blade may be resolved into a force and moment acting at the tip of the kth flexbeam. These are exactly balanced by structural loads that the kth flexbeam exerts at the root of the kth blade, since all aerodynamic and inertial loads along the flexbeam are neglected. The flexbeam structural loads are not expressible in closed form and require special treatment.

Flexbeam Structural Loads

The force vector $\boldsymbol{F}_k$ representing forces that the kth blade exerts on the kth flexbeam, and the moment vector, $\boldsymbol{M}_k$, representing the moments that the kth blade exerts on the kth flexbeam, have steady and unsteady components

$$\boldsymbol{F}_k = \boldsymbol{F} + \tilde{\boldsymbol{F}}_k(t)$$
$$\boldsymbol{M}_k = \boldsymbol{M} + \tilde{\boldsymbol{M}}_k(t) \tag{1}$$

Unsubscripted quantities are steady components; tilde quantities are unsteady components. Similarly,

$$u_k = u + \tilde{u}_k(t), \quad \zeta_k = \zeta + \tilde{\zeta}_k(t)$$
$$v_k = v + \tilde{v}_k(t), \quad \beta_k = \beta + \tilde{\beta}_k(t)$$
$$w_k = w + \tilde{w}_k(t), \quad \theta_k = \theta + \tilde{\theta}_k(t) \tag{2}$$

The steady components $\boldsymbol{F}$ and $\boldsymbol{M}$ depend nonlinearly on u,v,w,ζ,β,θ due to geometric nonlinearities. The unsteady components $\tilde{\boldsymbol{F}}_k$ and $\tilde{\boldsymbol{M}}_k$ may be linearized analytically in the following quantities and their first- and second-time derivatives: $\tilde{u}_k, \tilde{v}_k, \tilde{w}_k, \tilde{\zeta}_k, \tilde{\beta}_k, \tilde{\theta}_k, X, Y, \Phi_x, \Phi_y$.

Flexbeam Equilibrium Deflections

Let us consider first the flexbeam equilibrium deflections, the steady part of the solution. If u,v,w,ζ,β,θ were known, then $\boldsymbol{F}$ and $\boldsymbol{M}$ would be determined. If the forces and moments at the root of the flexbeam $\boldsymbol{F}_R$ and $\boldsymbol{M}_R$ were known, the geometrically exact curvature-slope-deflection relations could be numerically integrated along the flexbeam to obtain the correct tip deflections. This is a type of two-point boundary value problem involving relationships between the tip deflections and root forces and moments.

A practical scheme for the solution of this problem is given in the following seven steps:

1) Assume a set of flexbeam tip deflections $u_t, v_t, w_t, \zeta_t, \beta_t, \theta_t$.

2) Calculate the forces and moments $\boldsymbol{F}$ and $\boldsymbol{M}$ based on the assumed deflections.

3) Transfer the force and moment $\boldsymbol{F}$ and $\boldsymbol{M}$ to the equivalent root force and moment $\boldsymbol{F}_R$ and $\boldsymbol{M}_R$ using the assumed tip deflections.

4) Evaluate the tension force and bending torsion moments for a generic point along the flexbeam in terms of the local deflections and rotations along the deformed flexbeam.

5) Use linear moment-curvature relations and numerically integrate the geometrically exact expressions relating bending curvatures and twist to rotations and deflections.[14]

6) Compare the assumed tip deflections $u_t, v_t, w_t, \zeta_t, \beta_t, \theta_t$ with the tip deflections obtained from step 5.

7) Minimize

$$\mathfrak{F} = (u_t - u)^2 + (v_t - v)^2 + (w_t - w)^2 + (\zeta_t - \zeta)^2 + (\beta_t - \beta)^2 + (\theta_t - \theta)^2 \tag{3}$$

The miminum $\mathfrak{F} = 0$ is the exact solution to the equilibrium position of the rotor blades. This minimum can be found by use of the nonlinear least-squares algorithm of Levenberg-Marquardt.[17]

Flexbeam Perturbation Deflection

In addition to the equilibrium solution, we must also find the perturbation forces and moments that the flexbeam exerts on the blade root in response to perturbation deflections. This is done by numerically perturbing the equilibrium force and moment components in the directions of u,v,w,ζ,β,θ and recomputing the deflections. The results can be expressed symbolically as:

$$\begin{Bmatrix} \tilde{u}_k \\ \tilde{v}_k \\ \tilde{w}_k \\ \tilde{\zeta}_k \\ \tilde{\beta}_k \\ \tilde{\theta}_k \end{Bmatrix} = [F] \begin{Bmatrix} \tilde{F}_{u_k} \\ \tilde{F}_{v_k} \\ \tilde{F}_{w_k} \\ \tilde{M}_{\zeta_k} \\ \tilde{M}_{\beta_k} \\ \tilde{M}_{\theta_k} \end{Bmatrix} \tag{4}$$

where $[F]$ is a 6×6 matrix, identical for all k, the elements of which are

$$F_{ij} = \frac{\begin{pmatrix} i\text{th deflection due to } j\text{th perturbed load} \\ -i\text{th equilibrium deflection} \end{pmatrix}}{\epsilon} \tag{5}$$

and ϵ is the amount the loads are perturbed. The matrix elements F_{ij} are symmetric for infinitesimal ϵ. Numerically, however, ϵ cannot be any smaller than the square root of the relative error of the deflections. On the other hand, an ϵ too large will produce slight nonsymmetry in F_{ij} due to geometric nonlinearity. The force and moment response of the flexbeam to small perturbations of the deflection may be obtained from Eq. (4) by simply inverting $[F]$. The resulting matrix $[F]^{-1}$ is the structural stiffness matrix for the flexbeam. The perturbation flexbeam structural loads may now be combined with the unsteady perturbation forces and moments produced by pitch-control system, inertia, gravity, quasisteady aerodynamics, and body springs and dampers to complete the system equations of motion.

Linearized Perturbation Equations

When all the generalized forces associated with both blade and body degrees of freedom are linearized in $\tilde{u}_k, \tilde{v}_k, \tilde{w}_k, \tilde{\zeta}_k, \tilde{\beta}_k, \tilde{\theta}_k, X, Y, \Phi_x, \Phi_y$ and in their first- and second-time derivatives, there are terms with periodic coefficients involving $\sin\psi_k$ and $\cos\psi_k$. All of these may be removed by the multiblade coordinate transformation which transforms the blade equations from a coordinate system rotating with the blades to one fixed in the body.[18] The transformation yields, for rotors with three or more blades, rotor collective, differential collective, and cyclic modes. Only the rotor cyclic modes are coupled to the body motion X, Y, Φ_x, Φ_y; hence, the collective and differential collective modes are not included in the present analysis. The details of applying this transformation to the present problem are given in Ref. 14. The resulting sixteen linear ordinary differential equations with

constant coefficients can be written as a matrix equation:

$$[A]\{\ddot{x}\}+[B]\{\dot{x}\}+[C]\{x\}=0 \tag{6}$$

where $[A]$, $[B]$, and $[C]$ contain elements that depend on the system parameters and blade equilibrium deflections u,v,w,ζ,β,θ and where the elements of the column vector $\{x\}$ consist of the sixteen degrees of freedom $u_c,u_s,v_c,v_s,w_c,w_s,\zeta_c,\zeta_s,\beta_c,\beta_s,\theta_c,\theta_s,X,Y,\Phi_x,\Phi_y$, where the subscripts c and s indicate cosine and sine components of the cyclic modes. The matrices contain no small-angle assumptions or geometric approximations. Equation (6) is solved as a conventional eigenvalue problem.

Numerical Results and Discussion

The eigenvalues of interest are usually closely associated with the lead-lag motion. In case of fuselage motion, the low-frequency rotor cyclic lead-lag mode $(\Omega-\omega_\zeta)$ generally couples with the body motion to produce instabilities when $\omega_\zeta<\Omega$ and when $\Omega-\omega_\zeta$ is nearly equal to one of the body frequencies.

Numerical results for various hypothetical bearingless rotor configurations are presented in eigenvalue form. For the eigenvalues $s=-\sigma+i\omega$, the system is stable for $\sigma>0$ and unstable for $\sigma<0$. In most cases, σ is shown only for the lead-lag bending mode. Cases for which other modes have light damping are shown as well. For each of the four cases (I-IV), results are presented for hub-fixed motion (X,Y,Φ_x,Φ_y motion suppressed), damping vs blade pitch angle at the blade three-quarter radius $\theta_{3/4}\cong\theta_f+\theta_b+\theta$. The coupled rotor-body results are shown for cases II-IV according to subcases A and B. Subcase A is for coupled rotor-body motion in hovering flight for $\tilde{\Omega}$ varying and thrust equal to weight. For subcase A, the aircraft is assumed to be mounted on a gimballed test stand with X and Y motions suppressed. Subcase B is for coupled rotor-body motion when the aircraft is in ground contact at zero thrust with $\tilde{\Omega}$ varying.

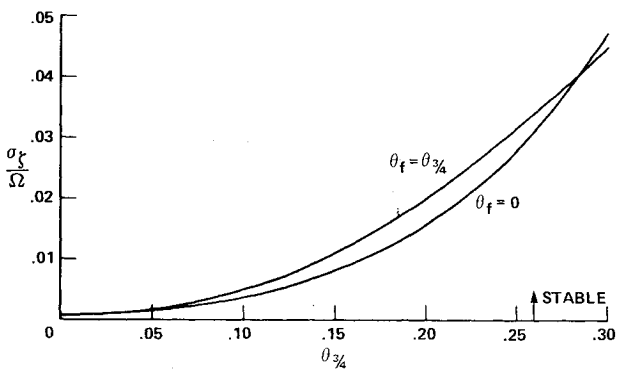

Fig. 5 Effect of flexbeam pitch angle on the lead-lag damping vs blade pitch angle, case I, hub-fixed.

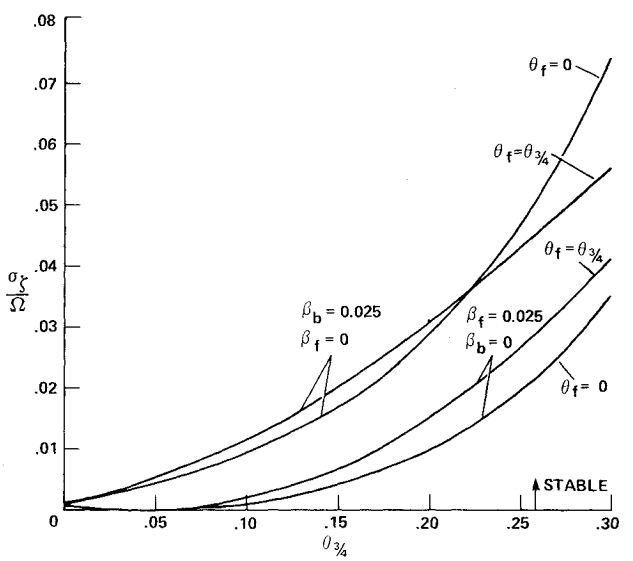

Fig. 6 Effect of blade and flexbeam precone on the lead-lag damping vs blade pitch angle, case I, hub-fixed.

Configuration Properties

The numerical results are generated for the nominal configuration as specified in Ref. 19, Tables 1-3. Due to space limitations, only parameters that depart from the nominal values are indicated in the figure captions. Parameters for the nominal case are believed to be suitable for approximately modeling a hypothetical soft in-plane bearingless rotor helicopter.

Isolated Blade Stability

The aeroelastic stability of an isolated blade rotating about an axis fixed in space has been treated extensively for hingeless rotors in hover and the design considerations for stability are reasonably well understood. For the bearingless rotor blade, however, very little information exists. Thus, we begin by looking at several configurations for cases I-IV as the pitch angle $\theta_{3/4}$ varies from 0-0.3 rad.

The damping σ_ζ vs pitch angle is shown for case I nominal in Fig. 5. The lead-lag frequency is about 0.7 Ω and the flap frequency is approximately 1.1 Ω. The torsion frequency varies among the different cases but is nominally near 2.5 Ω. The lead-lag damping for this configuration increases with an increase in pitch angle. This is typical of many soft in-plane hingeless rotors, as well.[11,12] The configuration marked $\theta_f=\theta_{3/4}$ is slightly more stable than the one marked $\theta_f=0$ for low to moderate values of $\theta_{3/4}$. This is due to the increased flap-lag coupling that comes from altering the structural principal axes in the flexbeam from essentially flat at $\theta_f=0$ to pitched up at $\theta_f=\theta_{3/4}$. Also, appreciable structural pitch-flap and pitch-lag coupling is possible in this configuration due to elastic deflection at equilibrium.

Depending on the built-in coning angles β_f and β_b and the amount of thrust, the effects of pitch-couplings may or may not stabilize the system. A comparison of Figs. 5 and 6 indicates that β_f is destabilizing and β_b is stabilizing for this configuration. As in case I, case II exhibits widely varying behavior in the presence of angular offsets. The effects of blade precone β_b are given in Fig. 7. That the system is

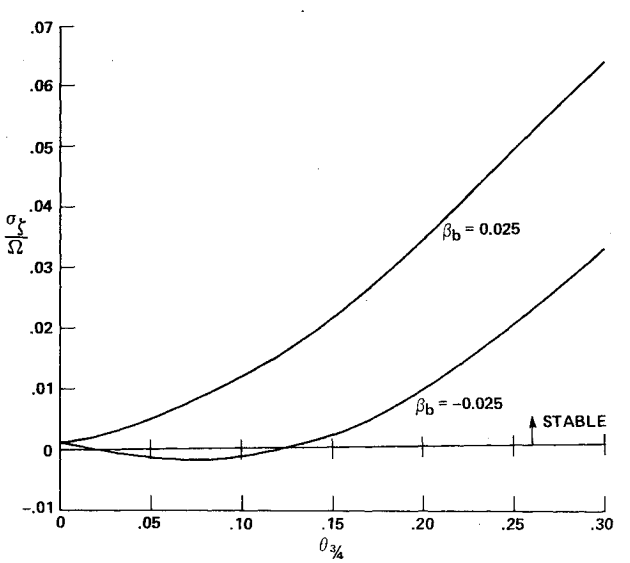

Fig. 7 Effects of blade precone on the lead-lag damping vs pitch angle, case II, hub-fixed.

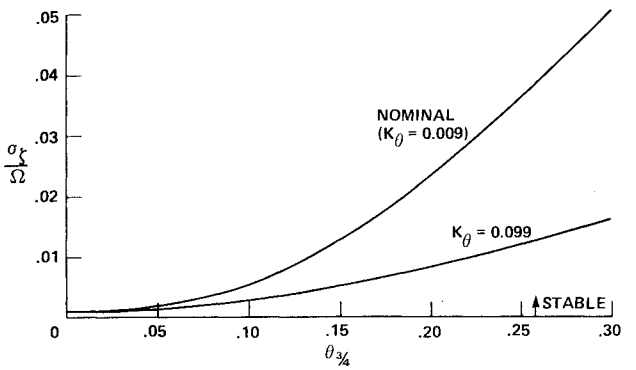

Fig. 8 Effect of torque tube stiffness on the lead-lag damping vs blade pitch angle, case II, hub-fixed.

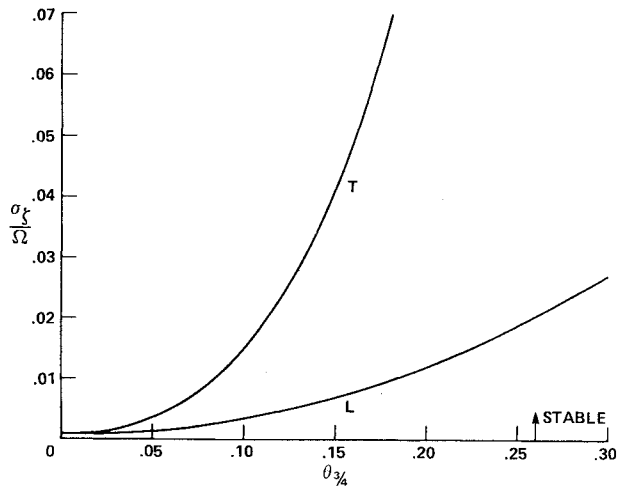

Fig. 9 Effect of pitch arm location on the lead-lag damping vs pitch angle, case III, hub-fixed, leading edge (L) and trailing edge (T) pitch arms.

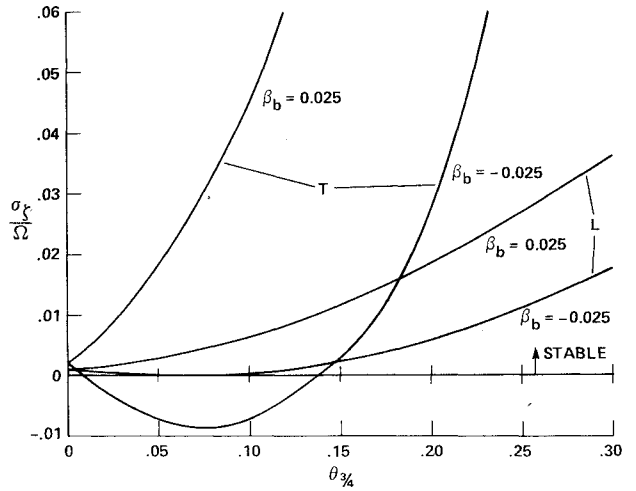

Fig. 10 Effect of blade and flexbeam precone on the lead-lag damping vs pitch angle, case III, hub-fixed, leading edge (L) and trailing edge (T) pitch arms.

stabilized by positive β_b is consistent with results obtained from the hingeless rotor analyses discussed in Refs. 5 and 12. An increase in the torsion stiffness will destabilize the nominal configuration, because the pitch-lag coupling will be diminished. This is confirmed in Fig. 8 where an increase in torque-tube torsion stiffness $\bar{K}_\theta$ from the nominal value of 0.009 to 0.099 is strongly destabilizing.

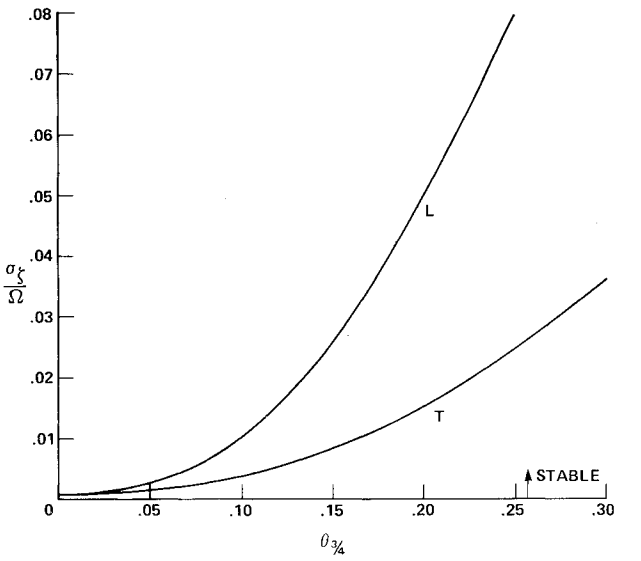

Fig. 11 Effect of inboard pitch arm location on the lead-lag damping vs pitch angle, case III, hub-fixed, leading edge (L) and trailing edge (T) pitch arms, $\bar{u}_I = 0$, $\bar{x}_I = -1$.

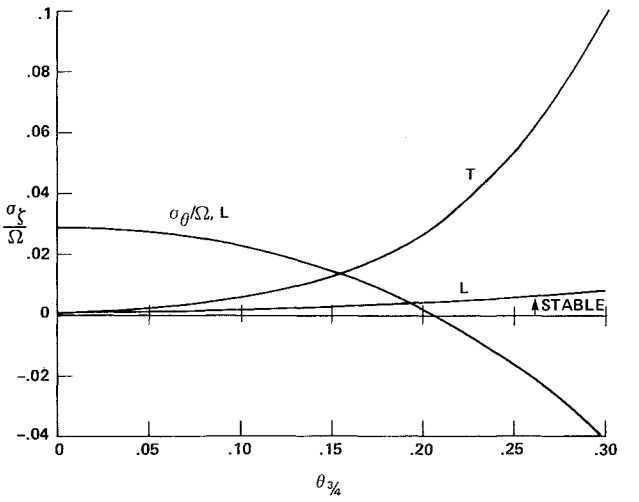

Fig. 12 Effect of snubber on the lead-lag damping vs pitch angle, case IV, hub-fixed, leading edge (L) and trailing edge (T) pitch arms (torsion mode damping also shown for L).

In the next series of figures, the effects of different pitch-control geometries are presented. Case III nominal is shown in Fig. 9. The *L* or *T* notation indicates the location of the pitch arm as either leading or trailing edge. The exact geometry is specified in Ref. 19. Due to a change in the sign of the pitch-lag and pitch-flap couplings, the trailing edge pitch arm is much more stable for this configuration. As in case II, case III indicates a strong sensitivity to β_b, as shown in Fig. 10. Notice that the damping is somewhat greater than for other cases at zero thrust for the trailing edge pitch arm with $\beta_b = 0.025$. When the pitch link is moved inboard, as in Fig. 11, the trends of stability are reversed, since the equivalent pitch-couplings change sign.

A snubber may be added to control the couplings in an attempt to reduce destabilizing effects. In Fig. 12, results are presented for case IV, nominal, identical to case III except that a snubber is added. The trailing edge pitch arm case is less stable than case III. However, for other configurations the opposite may be true; that is, a system with less stabilizing pitch coupling could be stabilized by the addition of a snubber.

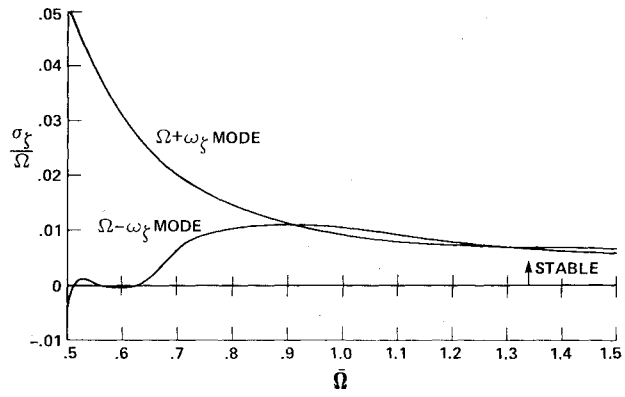

Fig. 13 Coupled rotor-body in hover lead-lag damping vs dimensionless rotor angular velocity, case IIA.

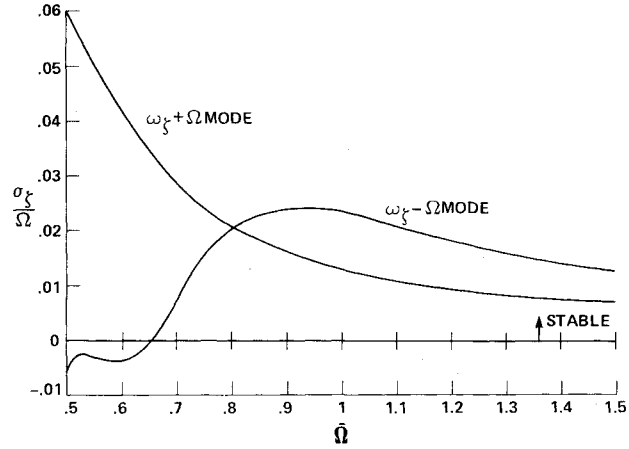

Fig. 14 Coupled rotor-body in hover lead-lag damping vs dimensionless rotor angular velocity, case IIA, $\beta_b = 0.025$.

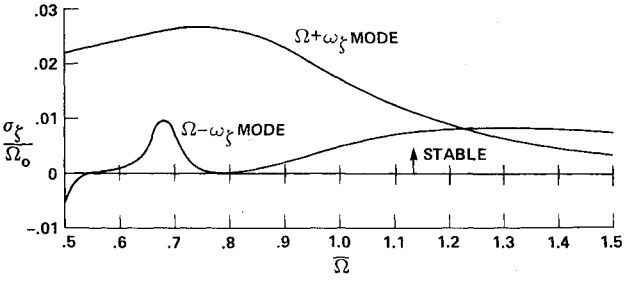

Fig. 15 Coupled rotor-body in hover lead-lag damping vs dimensionless rotor angular velocity, case IIIA, trailing edge (T) pitch arm.

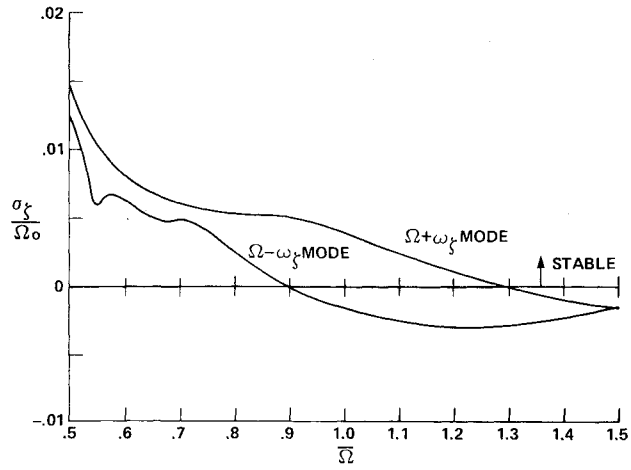

Fig. 16 Coupled rotor-body in hover lead-lag damping vs dimensionless rotor angular velocity, case IVA, trailing edge (T) pitch arm.

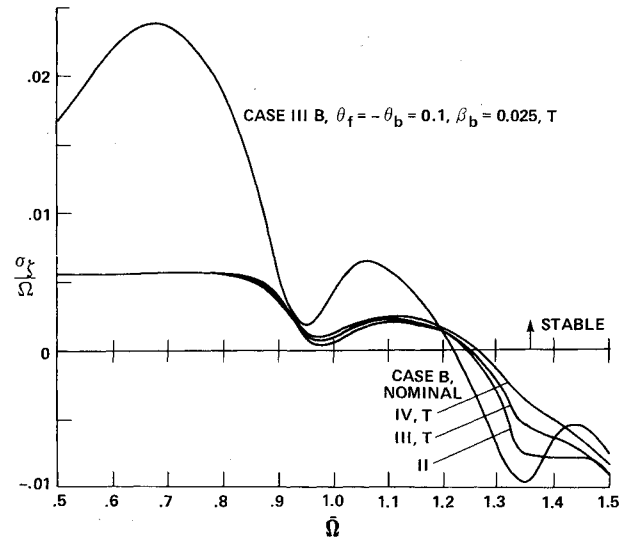

Fig. 17 Coupled rotor-body on ground lead-lag damping vs dimensionless rotor angular velocity, case IIB, IIIB(T), IVB(T), nominal, and case IIIB(T), $\theta_f = -\theta_b = 0.1$, $\beta_b = 0.025$.

Helicopter Aeromechanical Stability

When the body is free to interact dynamically with the rotor, air and ground resonance may occur. These instabilities, discussed by Ormiston,[5] stem mainly from mechanical and inertial considerations. They only occur with soft in-plane rotors, $\omega_\zeta < \Omega$, and generally appear when the low-frequency rotor lead-lag mode ($\Omega - \omega_\zeta$ mode) and the body mode frequencies are near coalescence. Only a few results for stability for the coupled rotor-body system in hover (air resonance) and on the ground (ground resonance) are given here.

Air Resonance

Rotor lead-lag mode $\Omega \pm \omega_\zeta$ dampings are shown for nominal case IIA in Fig. 13. Body coupling causes the two rotor mode dampings to differ; in the hub-fixed case these are identical to the isolated blade damping when there is no interblade coupling. As $\bar{\Omega}$ is changed, the system is unstable below $\bar{\Omega} = 0.632$ and the system damping appears to deteriorate as $\bar{\Omega}$ increases beyond $\bar{\Omega} = 1$.

Angular offsets may strongly influence stability, as shown in Fig. 14. The $\Omega - \omega_\zeta$ mode damping is almost doubled for $\bar{\Omega} > 0.9$, although instability occurs at a slightly higher $\bar{\Omega} = 0.652$.

The pitch-control geometry appears to have a significant effect on system stability. In Fig. 15, the trailing edge pitch arm case is shown without the snubber. The snubbed case of Fig. 16 is much less stable; one can only conclude that the effect of pitch-control geometry may be significant.

Ground Resonance

Cases IIB, IIIB(T), and IVB(T), nominal, and case IIIB(T) with $\theta_f = -\theta_b = 0.1$ and $\beta_b = 0.025$ are shown in Fig. 17. The stability boundary for ground resonance does not appear sensitive to the geometric or pitch-control parameters. It is possible, however, to increase the damping over the range of $\bar{\Omega}$, as shown by the curve $\theta_f = -\theta_b = 0.1$ and $\beta_b = 0.025$, but this is accompanied by a slight penalty in the crossing of the stability boundary. This is similar to the results obtained by Ormiston[5] who found it difficult to influence the stability of the system at zero thrust on the ground using aeroelastic couplings. It is well-known that ground resonance instability

can be suppressed by a certain amount of mechanical damping. It is not clear why an increase in damping obtained from the air will not stabilize the system.

Experimental Correlation

No correlation with experimental data is presented in this paper due to space limitations. The excellent correlation with two sets of experimental data in Ref. 20, however, indicates the potential utility of the analysis as a design tool.

Concluding Remarks

In this paper a theoretical technique for assessing the aeroelastic stability of bearingless rotors is presented. The analysis allows treatment of the geometric nonlinearities in the flexbeam and various pitch-control configurations while maintaining the simplicity of rigid-blade modeling. Numerical results are presented for a configuration believed to be representative of a hypothetical soft in-plane bearingless main rotor. The results indicate that an isolated blade in hover can usually be stabilized by properly choosing the angular offsets and pitch-control geometry. These parameters strongly influence the aeroelastic couplings and, in turn, the aeroelastic stability. When body motion is coupled to the rotor dynamics, the number of parameters is increased and the problem of stabilizing the design is more difficult. The results vary widely and it is not possible to draw many general conclusions.

References

[1] Donham, R. E., Cardinale, S. V., and Sachs, I. B., "Ground and Air Resonance Characteristics of Soft Inplane Rigid Rotor System," *Journal of the American Helicopter Society*, Vol. 14, Oct. 1969, pp. 33-41.

[2] Lytwyn, R. T., Miao, W., and Woitsch, W., "Airborne and Ground Resonance of Hingeless Rotor," Preprint 414, 26th Annual Forum of the American Helicopter Society, Washington, D.C., June 1970.

[3] Miao, W. and Huber, H. B., "Rotor Aeroelasticity Coupled with Helicopter Body Motion," NASA SP-352, Feb. 1974, pp. 137-146.

[4] Young, M. I., Bailey, D. J., and Hirschbein, M. S., "Open and Closed Loop Stability of Hingeless Rotor Helicopter Air and Ground Resonance," NASA SP-352, Feb. 1974, pp. 205-218.

[5] Ormiston, R. A., "Aeromechanical Stability of Soft Inplane Hingeless Rotor Helicopters," Paper 25, Third European Rotorcraft and Powered Lift Aircraft Forum, Aix-en-Provence, France, Sept. 1977.

[6] Bielawa, R. L., Cheney Jr., M. C., and Novak, R. C., "Investigation of a Bearingless Helicopter Rotor Concept Having a Composite Primary Structure," NASA CR-2637, 1976.

[7] Fenaughty, R. R. and Noehren, W. L., "Composite Bearingless Tail Rotor for UTTAS," Preprintg 1084, 32nd Annual Forum of the American Helicopter Society, Washington, D. C., May 1976.

[8] Harvey, K. W., "Aeroelastic Analysis of a Bearingless Rotor," Americal Helicopter Society Symposium on Rotor Technology, Essington, Pa., Aug. 1976.

[9] Shaw Jr., J. and Edwards, W. T., "The YUH-61A (UTTAS) Tail Rotor: The Development of a Stiff Inplane Bearingless Flexstrap Design," Preprint 77.33-32, 33rd Annual Forum of the American Helicopter Society, Washington, D.C., May 1977.

[10] Harris, F. D., Cancro, P. A., and Dixon, P.G.C., "The Bearingless Main Rotor," Paper 4, Third European Rotorcraft and Powered Lift Aircraft Forum, Aix-en-Provence, France, Sept. 1977.

[11] Hodges, D. H. and Ormiston, R. A., "Stability of Elastic Bending and Torsion of Uniform Cantilever Rotor Blades with Variable Structural Coupling," NASA TN D-8192, 1976.

[12] Hodges, D. H. and Ormiston, R. A., "Stability of Hingeless Rotor Blades in Hover with Pitch-Link Flexibility," *AIAA Journal*, Vol. 15, April 1977, pp. 476-482.

[13] Bielawa, R. L., "Aeroelastic Analysis for Helicopter Rotor Blades with Time Variable, Nonlinear Structural Twist and Multiple Structural Redundancy—Mathematical Derivation and Program User's Manual," NASA CR-2638, 1976.

[14] Hodges, D. H., "Aeromechanical Stability of Helicopters with a Bearingless Main Rotor—Part I: Equations of Motion," NASA TM-78459, 1978.

[15] Kane, T. R., *Dynamics*, Holt, Rinehart, and Winston, New York, 1968.

[16] Greenberg, J. M., "Airfoil Sinusoidal Motion in a Pulsating Stream," NACA TN-1326, 1947.

[17] Brown, K. M. and Dennis, J. E., "Derivative Free Analogues of the Levenberg-Marquardt and Gauss Algorithms for Nonlinear Least Square Approximations," *Numerische Mathematik*, Vol. 18, 1972, pp. 289-297.

[18] Hohenemser, K. H. and Yin, S. K., "Some Applications of the Method of Multiblade Coordinates," *Journal of the American Helicopter Society*, Vol. 17, July 1972, pp. 3-12.

[19] Hodges, D. H., "A Theoretical Technique for Analyzing Aeroelastic Stability of Bearingless Rotors," *Proceedings of the 19th Structures, Structural Dynamics and Materials Conference*, Bethesda, Md., April 1978, pp. 282-294.

[20] Hodges, D. H., "An Aeromechanical Stability Analysis for Bearingless Rotor Helicopters," *Journal of the American Helicopter Society*, Vol. 24, Jan. 1979, pp. 2-9.